Materials Today Bio 31 (2025) 101537

Contents lists available at ScienceDirect

Materials Today Bio

journal homepage: www.journals.elsevier.com/materials-today-bio

Chitin nanocrystal-reinforced chitin/collagen composite hydrogels for annulus fibrosus repair after discectomy

Mingzhi Liu [a,1], Zhiyong Cui [b,1], Derong Xu [a], Chenguang Liu [b,*], Chuanli Zhou [a,**]

[a] The Affiliated Hospital of Qingdao University, 266035, Qingdao, China
[b] College of Marine Life Sciences, Ocean University of China, 266003, Qingdao, China

ARTICLE INFO

Keywords:
Hydrogel patch
Annulus fibrosus defect repair
Chitin
Collagen
Chitin nanocrystal

ABSTRACT

Discectomy is a widely utilized approach for alleviating disc herniation; however, effective repair of postoperative annulus fibrosus (AF) defects remains a significant challenge. This study introduces a hydrogel patch with enhanced mechanical properties for AF repair fabricated using chitin (Ch), collagen (Col), and chitin nanocrystals (ChNCs) through a freeze-thaw cycling technique. The Ch and Col components constitute the matrix of the hydrogel patch, while uniformly dispersed ChNCs act as a nanofiller, markedly improving the mechanical performance (compression strain: 95 %; compression modulus: 0.27 MPa) of the resulting Ch/Col@ChNCs hydrogel patch. The patch demonstrates advantageous properties, including high porosity, superior water absorption, thermal stability, and biodegradability in simulated body fluid. In vitro assessments reveal excellent biocompatibility with AF cells and enhanced collagen deposition. Furthermore, in vivo studies confirm that the patch effectively repairs postoperative disc defects, exhibiting strong integration with surrounding tissues and facilitating the orderly regeneration of fibrous tissue. This innovative hydrogel patch, combining exceptional properties with a straightforward fabrication process, presents a viable strategy for advancing clinical biomaterials for postoperative AF repair.

1. Introduction

Lower back pain is the leading cause of disability globally [1,2], with Lumbar disc herniation being its most revalent underlying cause [3,4]. This condition is primarily attributed to intervertebral disc (IVD) degeneration (IDD) [5]. Degenerated discs experience significant structural changes, including reduced elasticity and hydration capacity of the nucleus pulposus (NP), alongside the formation of annulus fibrosus (AF) fissures. These changes compromise the stress-bearing capacity of the disc. Furthermore, the NP often breaches the AF and compresses adiacent spinal nerves, leading to pain and associated neurological symptoms [6,7]. In cases where conservative management fails, Surgical intervention becomes necessary to alleviate symptoms and restore function [8]. Discectomy is a widely used surgical technique that relieves nerve root compression by removing degenerated and herniated disc tissues, effectively addressing symptoms such as lower back pain [9]. However, this procedure leaves behind AF defects, which gradually form scar tissue. These defects allow NP material to reherniate easily, causing recurrent nerve compression and pain. Therefore, innovative strategies are critically needed to repair AF defects and restore NP hydration, aiming to improve long-term outcomes following discectomy [10].

Currently, physical sutures and rigid metallic implants are the primary materials utilized to address AF and NP issues [11]. While these materials can reduce the recurrence of surgeries, their application is largely limited to physical repairs and does not facilitate the biological healing of AF tissue [12,13].In contrast, tissue-engineering biomaterials have emerged as a promising approach for IVD repair [14,15]. These biomaterials can effectively seal postoperative AF defects while simultaneously promoting tissue healing and repair. Maintaining NP hydration prevents further IDD and significantly reduces the risk of reherniation following discectomy [16,17]. Various natural and synthetic biomaterials have been extensively investigated for annulus fibrosus (AF) repair. Natural biomaterials, such as collagen, chitosan, and alginate, are highly valued for their biocompatibility and resemblance to the native extracellular matrix (ECM).

* Corresponding author.
** Corresponding author.
E-mail addresses: liucg@ouc.edu.cn (C. Liu), justin_5257@hotmail.com (C. Zhou).
[1] These authors contributed equally.

https://doi.org/10.1016/j.mtbio.2025.101537
Received 25 October 2024; Received in revised form 6 January 2025; Accepted 1 February 2025
Available online 1 February 2025

In contrast, synthetic materials, including polycaprolactone (PCL), polyglycolic acid (PGA), and poly(lactic-co-glycolic acid) (PLGA), offer customizable mechanical properties and controlled degradation rates. These materials are often incorporated into hydrogels, scaffolds, or composite systems to provide structural support and facilitate tissue regeneration.For instance, porcine fibrin gels have been shown to enhance AF suture closure, maintain NP hydration, and delay the progression of postoperative IDD [18]. Similarly, Degradable polyglycolic acid–hyaluronan scaffold implants have demonstrated effectiveness in promoting AF repair in a sheep lumbar disc defect model [19]. Electrospun PCL-supported type I collagen (Col) hydrogels have also been utilized for AF repair and regeneration in degenerated IVD [20]. In addition, nanofiber scaffolds derived from collagen self-assembly and electrospinning closely mimic AF architecture, promoting AF cell proliferation, ECM secretion, and NP hydration [21]. Despite their advantages, natural hydrogels face limitations such as low mechanical strength, which can lead to material displacement and compromised structural integrity. Furthermore, their production often involves complex manufacturing processes that rely on toxic crosslinking agents, presenting significant obstacles to clinical translation [22].

Nanomaterials have been extensively evaluated as delivery systems for IVD repair. However, their complex designs limit their potential for clinical translation [23,24]. Despite this, nanomaterials can be utilized to enhance the mechanical properties of other materials. For instance, while chitosan is a natural and soft biomaterial, its inherent elasticity is insufficient to effectively repair AF. To address this limitation, Cellulose nanofibers have been incorporated into chitosan hydrogels to improve their mechanical properties, making them more suitable for repairing AF defects and providing enhanced support for AF regeneration [25]. Nevertheless, a mismatch persists between the material composition and the structural and functional requirements of the fibrous ring. Despite significant advancements in AF repair, developing a biomaterial that simultaneously satisfies the mechanical and biological demands of AF repair while ensuring clinical applicability remains a formidable challenge. Existing solutions frequently fail to provide the necessary mechanical support and to facilitate effective tissue regeneration.

Chitin (Ch) is a natural marine polysaccharide found in crustacean shells and fungal cell walls. It offers several advantages, including nontoxicity, nonimmunogenicity, and biocompatibility, making it a valuable material for biomedical applications [26]. Additionally, Ch can be processed into nanofibers [27]. It is commonly employed in fabricating three-dimensional (3D) hydrogels to support cell growth by providing attachment points for cells, although its structural limitations necessitate combination with other materials [28,29]. Collagen (Col), the primary ECM protein in the human body, offers excellent biocompatibility, high porosity, and ease of processing, making it an ideal candidate for tissue-engineering scaffolds [30]. Specifically, Type I Col, a major component of AF tissue, forms fibrous structures that impart elasticity to the AF, which can compensate for the limitations of Ch as a biomaterial [31]. Chitin nanocrystals (ChNCs), characterized by their highly ordered crystalline structure, exhibit exceptional mechanical properties, including high strength and stiffness, significantly enhancing composite materials' mechanical performance. Consequently, ChNCs are increasingly recognized as key components in developing advanced tissue -engineering biomaterials [32]. Research has demonstrated that incorporating ChNCs into hydrogel composites substantially improves the mechanical properties of the chitosan hydrogel network [33].

Furthermore, studies have shown that ChNCs promote the ordered aggregation of protein molecules by improving molecular conformations. This process involves the transformation of α-helices into β-sheets, the exposure of tryptophan residues, and an increase in overall crystallinity, which collectively enhance the structural integrity of the material. The inclusion of ChNCs within hydrogel systems enhances mechanical properties through increased hydrophobic interactions, electrostatic interactions, and hydrogen bonding within the gel matrix [34]. Consequently, the combination of Ch, Col, and ChNCs is anticipated to produce a composite hydrogel that synergistically integrates the structural and biological advantages of each component. This hydrogel is expected to exhibit excellent biocompatibility and mechanical strength by leveraging simple physical interactions, making it highly suitable for IVD repair applications.

In this study, a composite hydrogel incorporating chitin Ch, Col, and ChNCs, referred to as Ch/Col@ChNCs, was developed to overcome the limitations of existing materials for AF repair. Building on our prior success with chitosan–hydroxyapatite–collagen composite scaffold for tibial defect repair [35], the mechanical strength of this hydrogel was significantly improved by the addition of ChNCs (Fig. 1). The efficacy of the hydrogel in promoting AF repair was assessed through a combination of in vitro cell experiments and in vivo animal studies, which confirmed its feasibility and therapeutic potential. This study offers a promising and straightforward approach for developing biomaterial-based solutions to address AF defects and reduce the risk of IVD reherniation, potentially paving the way for innovative clinical strategies.

2. Materials and methods

2.1. Materials

Chitin (Ch; CAS 1398-61-4) was purchased from Qingdao Red Sea Biotechnology Co., Ltd. (Qingdao, China), and collagen (Col; CAS 9064-67-9) was obtained from Kramar Company (Shanghai, China). Human annulus fibrosus (AF) cells (HUM-iCELL-s012) were sourced from Saibaikang Biotechnology Co., Ltd. (Shanghai, China). Jinan Pengyue Experimental Animal Breeding Co., Ltd. (Jinan, China) provided New Zealand white rabbits for use in this study. All other reagents utilized in the experiments were commercially available and of analytical grade.

2.2. Preparation of Ch/Col@ChNCs composite hydrogels

Ch powder was dissolved in a solution containing 3.5 M KOH and 0.6 M urea and subjected to repeated freeze-thaw cycles at −80 °C and 25 °C to produce a 4 % Ch solution. Separately, Col was dissolved in 0.05 M acetic acid to prepare a 4 mg/mL Col solution. The Ch solution was dialyzed against deionized water at 37 °C to form the chitin hydrogel (Ch-gel). A composite hydrogel of Ch and Col (Ch/Col-gel) was prepared by mixing the Ch and Col solutions in a 3:1 vol ratio and dialyzing the mixture in deionized water at 37 °C. Chitin nanocrystals (ChNCs), prepared using the method described in the Supporting Information, were suspended in the Ch/Col solution (V_{Ch}:V_{Col} = 3:1) and ultrasonicated at 40 % power with 2-s intervals for 5 min. This process produced a 0.5 % ChNCs suspension (Fig. 1) [36]. The suspension was subsequently dialyzed against deionized water at 37 °C for 24 h, resulting in the final chitin nanocrystal-enhanced collagen/chitin composite hydrogel (Ch/Col@ChNCs-gel).

2.3. ChNCs characterization

Copper grids were coated with the ChNCs suspension, and one side of the grid was placed on a staining solution for 3 min, followed by air drying for an additional 3 min [33]. This process was repeated three times to ensure uniform staining. After complete drying, images were captured using a transmission electron microscope (TEM) (DU-650, BECKMAN Co., USA). To prepare a 0.5 % ChNCs suspension, ChNCs powder was dispersed in deionized water and ultrasonicated for 5 min at 40 % power with 2-s intervals. The zeta potential of the ChNCs under neutral conditions was measured using a laser particle-size analyzer (Nano ZS90, Malvern Instruments LimitedUK) [37].

2.4. Ch/Col@ChNCs composite hydrogel characterization

The characterization of the Ch/Col@ChNC composite hydrogel,

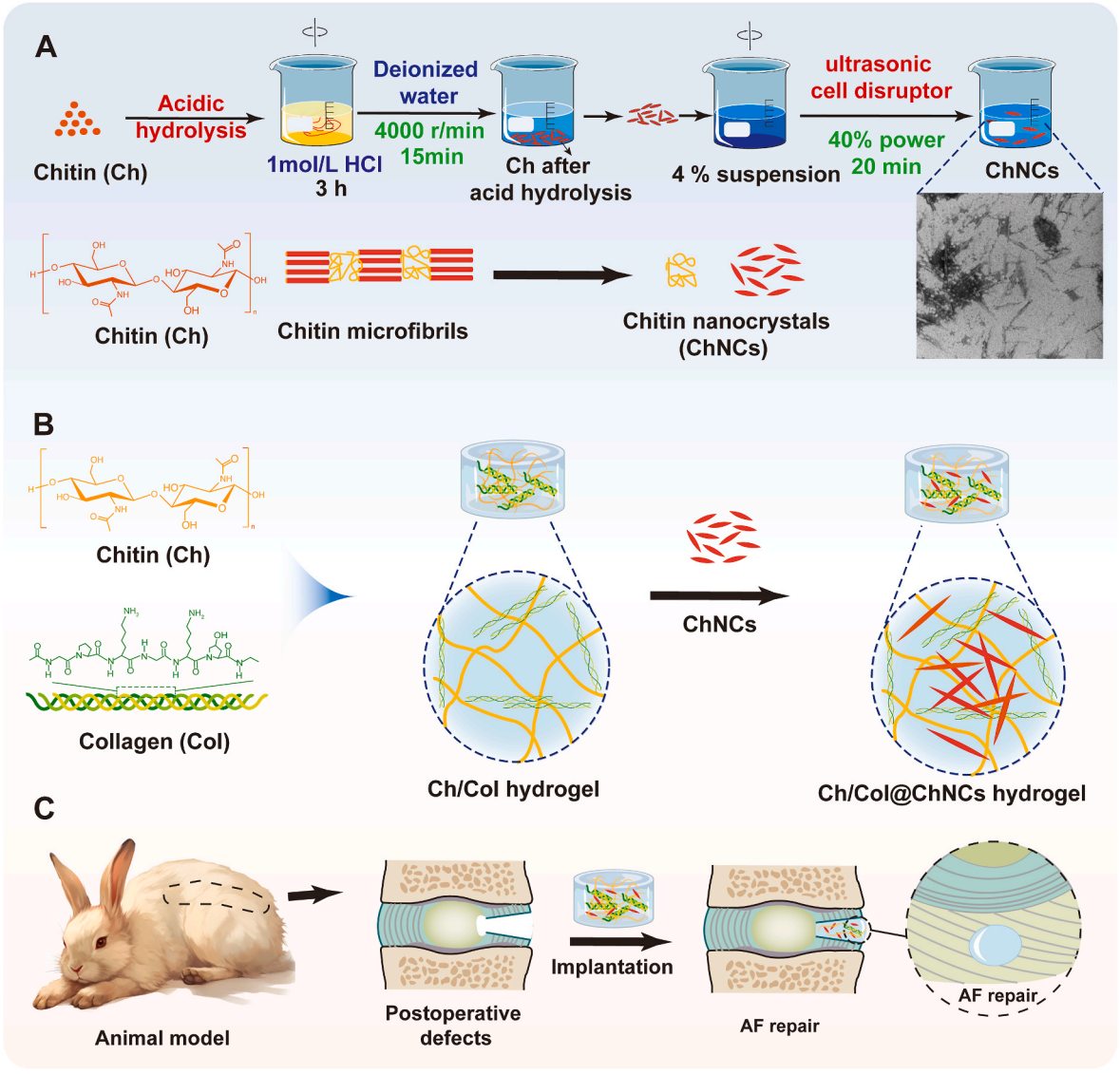

Fig. 1. Schematic of the ChNCs-reinforced Ch/Col composite hydrogels (Ch/Col@ChNCs) for postoperative AF repair. (A) Preparation of ChNCs, (B) Preparation of Ch/Col@ChNCs hydrogels, (C) The schematic of the AF postoperative repair.

including structural analysis, phase composition, thermal stability, mechanical properties, microstructure, porosity, and water-absorption rate, is provided in the Supporting Information.

2.5. *In vitro biocompatibility evaluation*

Ch-gel, Ch/Col-gel, and Ch/Col@ChNCs hydrogels were sterilized under ultraviolet (UV) light and cultured in a complete medium for 1, 3, and 7 days. The viability of human annulus fibrosus cells (hAFCs) grown on the hydrogel surfaces was assessed using a Cell Counting Kit-8 (CCK-8) assay, and absorbance was measured at 450 nm using a microplate reader (Multiskan Go 1510, Thermo Fisher Scientific Inc., USA). hAFC viability and cytotoxicity were further evaluated using the Propidium Iodide (Calcein/PI) Cell Viability/Cytotoxicity Assay Kit and observed under an inverted fluorescence microscope. Live cells stained green with Acetoxymethyl Ester (Calcein AM) were detected under excitation at 488 nm, while dead cells stained red with propidium iodide (PI) were observed under excitation at 555 nm [38]. The methods for blood-compatibility testing and extracellular matrix (ECM) deposition analysis are detailed in the Supporting Information.

2.6. *In vivo efficacy evaluation of Ch/Col@ChNCs*

The experiment included 12 healthy male New Zealand rabbits aged three months, with body weights ranging from 1.0 to 1.5 kg. The rabbits were sourced from the Animal Center of Qingdao University, and all Animal experiments were approved by the Animal Ethics Review Committee of Qingdao University (Approval No. 20240229NZR1220240610074). The procedures adhered to the ARRIVE guidelines and were conducted in compliance with the U.K. Animals (Scientific Procedures) Act, 1986, and associated guidelines, as well as the EU Directive 2010/63/EU for animal experiments. After 12 h of fasting and water deprivation, the rabbits received pretreatment with atropine injections, followed by anesthesia with sodium pentobarbital and local lidocaine administration. The intervertebral disc (IVD) segments were identified based on palpable spinous processes, and the L3–L6 discs were exposed using a posterolateral approach. The discs were divided into three groups: control (L3/4), untreated (L4/5), and treatment (L5/6). For The untreated and treatment groups, AF defect models were created by puncturing the discs with an 18G needle to a depth of approximately 5 mm, while healthy discs served as controls. In the treatment group, the defects were filled with sterile Ch/Col@ChNCs

hydrogels. The wounds were irrigated and sutured in layers, and infection prophylaxis was administered with 800,000-unit injections of penicillin sodium for three consecutive days. The wounds were disinfected with iodophor, and the dressings were changed every three days for a total of three changes [39]. Detailed methods for magnetic resonance imaging (MRI) and histological analyses are provided in the Supporting Information.

2.7. Statistical analysis

All quantitative data are presented as the mean ± standard deviation (SD). Differences between study groups were analyzed using one-way analysis of variance (ANOVA) followed by multiple comparison tests by Newman–Keuls. A p -value of <0.05 was considered statistically significant. All statistical analyses were performed using GraphPad Prism 9.

3. Results

3.1. Preparation and characterization of ChNCs

As shown in Fig. 2A, chitin nanocrystals (ChNCs) were prepared through acid hydrolysis, a process that involves the selective cleavage of β-1,4-glycosidic bonds in the amorphous regions of chitin. This step effectively removes the non-crystalline domains. ultrasonic treatment was subsequently applied to separate the amorphous and crystalline regions and promote the dispersion of ChNCs [32]. The ChNCs interact with the hydrogel via hydrogen bonding. The morphology of ChNCs, illustrated in Fig. 2B, reveals sharp, elongated, needle-like structures that are uniformly dispersed without visible aggregation. The average length and diameter of the ChNCs, as shown in Fig. 2C and detailed in Table S2, are 272.01 ± 40 nm and 14 ± 3 nm, respectively, consistent with previously reported values for ChNCs [27,33,40,41]. A high aspect ratio of 19.43 was calculated, indicating the suitability of the material for reinforcement applications. The zeta potential of ChNCs under neutral conditions was measured as (36 ± 0.8) mV, with an absolute value exceeding 30, indicating a relatively stable suspension. This stability is primarily due to the protonation of the cationic amino groups on ChNCs under acidic conditions, which generates electrostatic repulsion [41–44]. The higher zeta potential helps prevent the aggregation of ChNCs particles, ensuring uniform dispersion. This stable dispersion is critical for enhancing the mechanical properties of the hydrogel, thereby ensuring its structural integrity and mechanical performance in practical applications. In summary, the characterization of the zeta potential not only provides a theoretical foundation for optimizing the mechanical properties of the hydrogel but also establishes the utility of ChNCs as reinforcing fillers for composite hydrogels.

3.2. Preparation and characterization of Ch/Col@ChNC

The Ch/Col hydrogel matrix was prepared by dialysis, and ChNCs suspension was subsequently added to form the Ch/Col@ChNCs composite hydrogel (Fig. 1). Fourier transform infrared (FTIR) spectroscopy was employed to characterize the chemical structures of the hydrogels (Fig. 2D). The spectrum of The Ch-gel exhibited characteristic Ch absorption peaks, consistent with previously reported values [34,45]. The introduction of Col into the Ch-gel matrix led to the appearance of both Ch and Col peaks, including a peak at 1255 cm^{-1} in the spectrum. Following the addition of ChNCs, the intensities of the amide I (1652 cm^{-1}), amide II (1567 cm^{-1}), and amide III (1380 cm^{-1}) bands were enhanced [46], indicating hydrogen bond (H bond) formation between the N–H groups of Ch and the C=O groups of Col. The small size and large surface area of ChNCs facilitate these interactions, explaining the increased intensity of the amide II and III bands in the Ch/Col@ChNCs

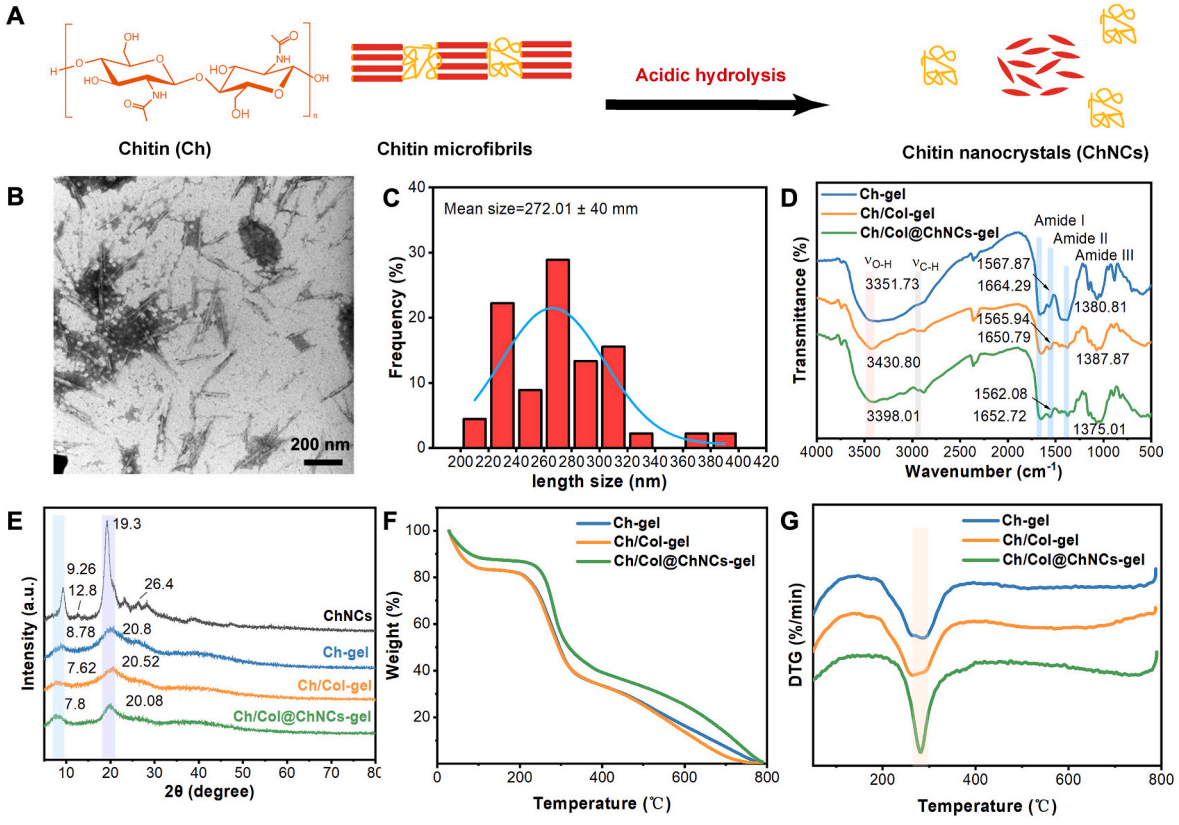

Fig. 2. ChNC structure and Characterization results of Ch-gel, Ch/Col-gel, and Ch/Col@ChNCs: (A) preparation scheme, (B) TEM image, (C) particle-size distribution, (D) FTIR spectra, (E) XRD patterns, (F) TG curves, and (G) DTG curves.

composite hydrogel [47]. This enhancement in H bonding validates the role of ChNCs in reinforcing the composite hydrogel.

The X-ray diffraction (XRD) patterns of ChNCs, Ch-gel, Ch/Col-gel, and Ch/Col@ChNCs structures are shown in Fig. 2E. The spectrum of ChNCs, characterized by a highly ordered crystalline structure, exhibited prominent peaks at 2θ values of 9.3° and 19.3°, indicative of strong hydrogen bonding and van der Waals interactions [48]. In contrast, the spectrum of Ch/Col-gel, which contains relatively more amorphous regions, displayed weaker and less distinct peaks [46]. These structural differences significantly influence the mechanical properties of the hydrogels, a critical factor for tissue engineering applications. High crystallinity enhances mechanical strength, whereas increased amorphous regions can diminish it [49]. The incorporation of ChNCs markedly improved the crystallinity of the hydrogel matrix, thereby enhancing its suitability for IVD implantation.

The thermal stabilities of the hydrogels were evaluated using thermogravimetric analysis (TGA, Fig. 2F). At 100 °C, the observed hydrogel mass loss was attributed to water evaporation [43]. The decomposition of Ch-gel and Ch/Col-gel began at 180 °C, primarily due to the thermal degradation of Ch and Col. In contrast, Ch/Col@ChNCs exhibited delayed decomposition at 210 °C [50]. This delay arises from two key factors: the tighter molecular packing within the ordered nanocrystals reduces the thermal decomposition rate, and the formation of additional hydrogen bonds (H bonds) with collagen (Col) and chitin (Ch) increases the decomposition temperature. Differential thermogravimetric (DTG) analysis (Fig. 2G) reveals that the maximum decomposition temperature of all samples occurs at approximately 280 °C. The more prominent maximum decomposition of Ch/Col-gel can be attributed to the lower thermal stability of Col [51]. In contrast, the higher maximum decomposition temperature observed for Ch/Col@ChNCs demonstrates that the incorporation of ChNCs significantly enhanced thermal stability [44]. These findings indicate that Ch/Col@ChNCs exhibit superior performance compared to the natural Ch/Col hydrogel matrix.

3.3. Compressive properties

The compressive properties of the hydrogel samples were tested to evaluate their mechanical performance. Fig. 3A illustrates the maximum deformation of 60 % for the Ch-gel. In Ch/Col-gel, the flexibility provided by the introduced Col network intertwines with the rigid Ch structure, enhancing the deformation capability of the hydrogel to 90 % and improving its resistance to deformation [52]. The Ch-gel itself withstands a maximum stress of 1.54 MPa. However, the introduction of Col to form Ch/Col-gelreduces the stiffness of the network due to increased elasticity, leading to cracks and fragmentation at maximum stress of 0.50 MPa. In contrast, the Ch/Col@ChNCs-gel achieves a maximum strain of 96 %, retaining the excellent elasticity of Ch/Col-gel while withstanding a maximum stress of 1.33 MPa, thereby compensating for the reduction in mechanical strength observed in Ch/Col-gel.

Fig. 3B highlights the significant variations in the compressive modulus of the hydrogel samples. The Ch-gel has a compressive modulus of 0.14 MPa, while the introduction of Col results in a modulus of 0.12 MPa, indicating no significant change. In contrast, incorporating ChNCs into Ch/Col@ChNCs-gel increases the modulus to 0.27 MPa, representing a 93 % enhancement over Ch-gel. This increase is attributed to the reinforcing effect of nanocrystals, which form additional crosslinking points [53]. In the Ch/Col@ChNC-gel, the uniform dispersion of ChNCs within the Ch/Col matrix creates rigid components that contribute to the overall structural integrity. Under compression, the hydrogel polymer network undergoes elastic deformation, aligning the

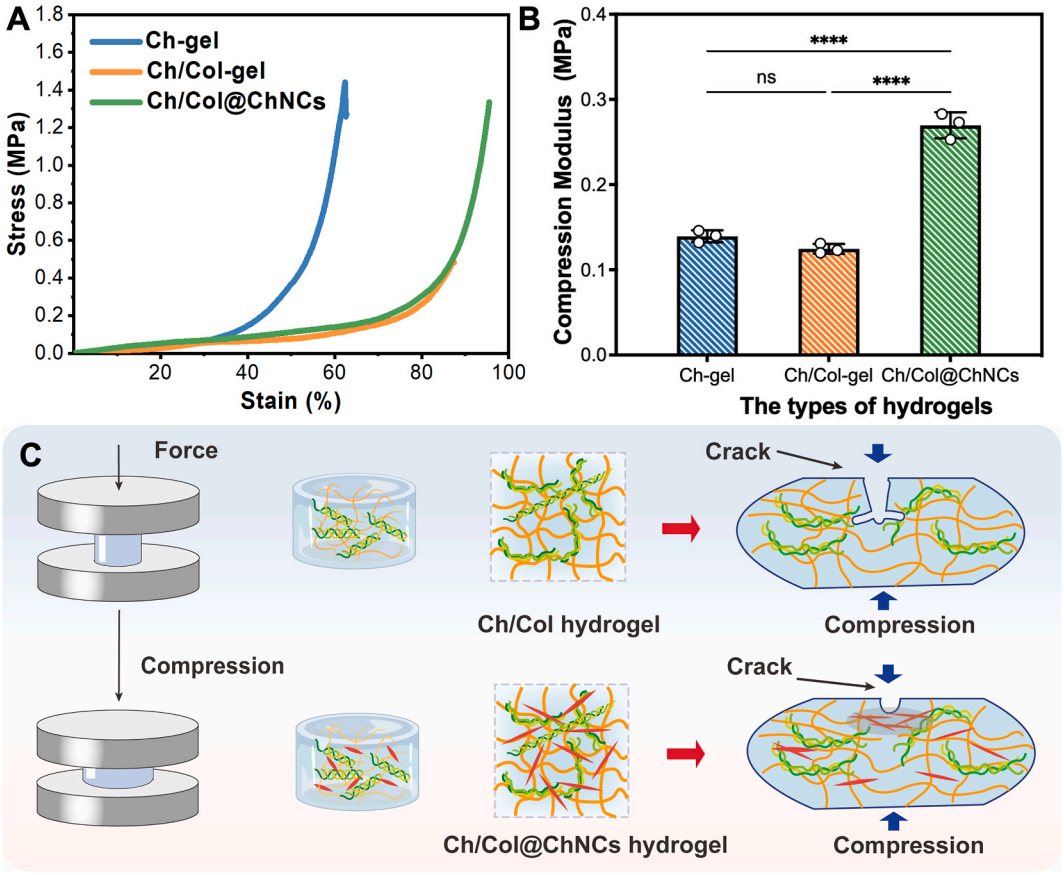

Fig. 3. Compressive properties of Ch-gel, Ch/Col-gel, and Ch/Col@ChNCs: (A) stress–strain curves, (B) elastic modulus, and (C) schematic of ChNCs introduction for enhanced compressive modulus (n = 3). Data are shown as mean ± SD; *$p < 0.05$, **$p < 0.01$, ***$p < 0.001$, ****$p < 0.0001$.

ChNC clusters and fibers along the compression axis due to their higher modulus compared to the polymer matrix. Upon unloading, the elasticity of the Ch/Col network facilitates the restoration of ChNC alignment [54]. Additionally, In Ch/Col@ChNC-gel with pre-existing cracks, the aligned ChNC clusters effectively transfer stress from the crack tips, reducing stress concentration and promoting crack deflection (Fig. 3C). This mechanism enhances the resistance of hydrogel to crack propagation, mimicking the behavior of AF under cyclic loading conditions [55].

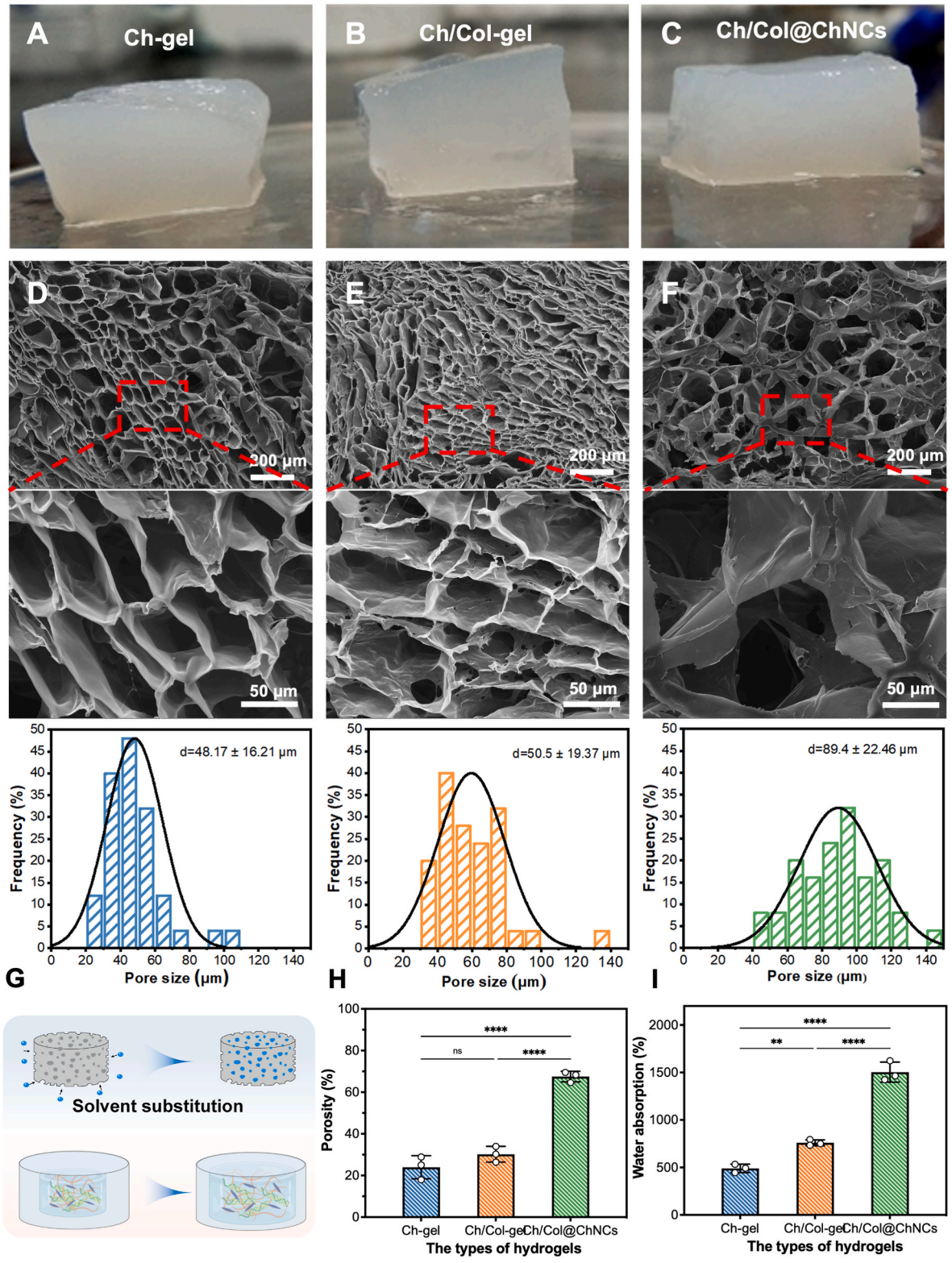

Fig. 4. Structural characterization of Ch-gel, Ch/Col-gel, and Ch/Col@ChNCs. (A, B, C) Optical images of Ch-gel, Ch/Col-gel, and Ch/Col@ChNCs hydrogels. (D, E, F) SEM images (200 × and 1000 ×) and pore size of Ch-gel, Ch/Col-gel and Ch/Col@ChNCs. The red dotted boxes represent the enlarged part. (G) Schematic of the testing principles for hydrogel porosity and water absorption, (H) porosity and (I) water absorption ratio of different hydrogels (n = 3). Data are shown as mean ± SD; $^{*}p < 0.05$, $^{**}p < 0.01$, $^{***}p < 0.001$, $^{****}p < 0.0001$.

Thus, the incorporation of ChNCs significantly enhances the mechanical properties of the natural hydrogel, aligning its mechanical performance with the requirements for IVD applications.

3.4. Morphology of hydrogels

Fig. 4A–C illustrates the appearance of three distinct gel samples: Ch-gel, with a smooth and translucent structure; Ch/Col-gel, showing increased opacity; and Ch/Col@ChNCs, exhibiting optimal opacity and a dense texture, which indicates the successful incorporation of chitin nanocrystals. The internal structures of the hydrogels were observed using scanning electron microscopy (SEM) after freeze-drying.

The SEM images show that all freeze-dried gels exhibit a porous structure (Fig. 4D–F). Among the three types, the pure Ch-gel (Fig. 4D) has the most compact pore structure, with an average pore size of 48.17 ± 16.21 μm. It features solid and complete pore walls with no apparent interconnectivity between pores, which is unfavorable for cell infiltration and migration. The Ch/Col-gel (Fig. 4E) also possesses a relatively compact pore structure, with an average pore size of 50.05 ± 19.37 μm. some pore walls contain holes, increasing interconnectivity between pores. The fibrous structure of collagen is observable in the cross-section, a result of collagen introduction. This structural change improves biocompatibility and enhances cell adhesion [35]. The Ch/Col@ChNCs hydrogel (Fig. 4F) has larger pore sizes, averaging 89.40 ± 22.46 μm, due to the introduction of ChNCs into the natural hydrogel matrix. This larger pore size is expected to improve water absorption. Furthermore, The specific cell adhesion properties of collagen promote cell attachment, while the crystalline structure and surface charge of ChNCs further enhance cell adhesion. The interconnected structure of the Ch/Col@ChNCs hydrogel creates an optimal environment for cell infiltration, proliferation, and migration, fulfilling the requirements for tissue engineering scaffolds [56].

3.5. Porosity and water absorption

We measured the porosity (Fig. 4H) and water absorption capacity (Fig. 4I) of the three hydrogels to evaluate the impact of ChNCs on these properties. A clear trend was observed: the porosity increased from 21 % in the Ch-gel to 30 % in the Ch/Col-gel and significantly to 67 % in the Ch/Col@ChNCs hydrogel. This finding suggests that ChNCs play a crucial role in enhancing porosity, aligning with the observations from the SEM results. The nanoscale crystalline structure and charge distribution of ChNCs likely contribute to creating additional voids and promoting the formation of larger pores within the hydrogel matrix, thereby increasing porosity [57].

Similar to the porosity behavior, the water absorption capacity of the hydrogels increases progressively across the three types. The Ch-gel exhibits a water absorption ratio of 4.8 times its dry weight, while the Ch/Col-gel demonstrates a higher absorption ratio of 7.6 times its dry weight. The most significant water absorption capacity was observed in the Ch/Col@ChNCs hydrogel, which absorbed up to 15 times its dry weight. This remarkable increase can be attributed to the high porosity and synergistic effects of Ch, Col, and ChNCs. The interconnected pores formed by the Ch, Col, and ChNC structures provide abundant space for water molecules to infiltrate the hydrogel matrix, while the electrostatic interactions and numerous adsorption sites within the structure facilitate water retention [58]. These findings emphasize the influence of hydrogel structure on its functional properties. The introduction of ChNCs and the interactions between Col and Ch not only increased porosity but also significantly enhanced the waterabsorption capacity of the hydrogels. This excellent water absorption property mimics the characteristics of NP and AF in IVD, which are essential for promoting AF repair. By absorbing moisture within tissues, the hydrogels can facilitate tissue regeneration and maintain NP hydration [7].

3.6. Biodegradability and stability analysis

The stability and biodegradability of hydrogels are critical parameters for their application in tissue engineering.The degradation of the hydrogels was evaluated both in vitro and in simulated in vivo environments, providing comprehensive insights into their stability and biodegradability. Ch is inherently biodegradable in vivo due to the enzymatic degradation of its β-(1 → 4)-glycosidic bonds by lysozyme [59,60]. Lysozyme, a cationic protein, is abundantly present in various body fluids such as urine, serum, saliva, and tears [61], with concentrations ranging from approximately 2 μg/L in urine to 2 mg/L in serum. To mimic the in vivo degradation environment, We prepared a simulated body fluid with a lysozyme concentration of 1.5 μg/mL. Phosphate-buffered saline (PBS) was used as the control to simulate the in vitro environment. Additionally, different pH values were employed to represent varying degenerative conditions similar to those found in IVD microenvironments.

We monitored the mass loss of the hydrogels at 37 °C over four weeks in both environments, assessing stability and degradation at specified intervals. As shown in Fig. 5A and D, the Ch-gel exhibited continuous mass loss in vitro, with no significant differences observed across pH values. In the simulated in vivo environment, over 50 % of the mass was lost on the first day, with no significant differences across pH values, contrasting with the in vitro environment. This accelerated degradation can be attributed to lysozyme breaking down the β-(1 → 4)-glycosidic bonds in the Ch chain, indicating that Ch-gel is less stable in vivo. As depicted in Fig. 5B and E, the Ch/Col-gel exhibited significantly lower mass loss than Ch-gel, with Approximately 20 % mass loss occurring within the first three days and no significant differences between the in vitro and in vivo environments. In contrast, As shown in Fig. 5C and F, Ch/Col@ChNCs initially maintained relative stability, with almost no mass loss before day 19. however, degradation began in the simulated in vivo environment, resulting in approximately 30 % mass loss by the fourth week. When Comparing the degradation profiles of the hydrogels over four weeks, Ch/Col@ChNCs demonstrated relative stability during the initial stages, followed by controlled biodegradation at an appropriate time. This behavior aligns with its mechanical strength and thermal stability, making it particularly advantageous for post-disc surgery recovery. the hydrogel can provide structural support within AF during the early healing phase and gradually degrade as tissue regeneration occurs, ultimately being replaced by native tissue.

3.7. Hemolysis assay for evaluating biocompatibility

A hemolysis assay was conducted to evaluate the biocompatibility of the hydrogels and determine their suitability for biomedical applications involving direct blood contact [62]. As shown in Fig. 6A, all hydrogels exhibited hemolysis rates below 5 % when normalized to the Triton group, which served as the positive control. In Fig. 6B, the supernatants of the hydrogel groups display a light-yellow color, similar to the PBS control group, in contrast to the red color observed in the Triton group. These results indicate that the hydrogels possess excellent biocompatibility and meet the acceptable standards for blood-contacting biomaterials, as defined by ISO 10993-4 [63].

Following the hemolysis test, red blood cells were resuspended for morphological analysis using an optical microscope. Fig. 6B highlights severe cell rupture and debris in the Triton group, emphasizing its cytotoxicity. In contrast, red blood cells in all hydrogel groups retained their circular shape without rupture, consistent with the morphology observed in the PBS group. This finding further validates the biocompatibility of the hydrogels, demonstrating no significant damage to cell membranes [64]. The low hemolysis rate and preserved red blood cell morphology highlight the excellent biocompatibility of the hydrogels for direct blood-contact applications.

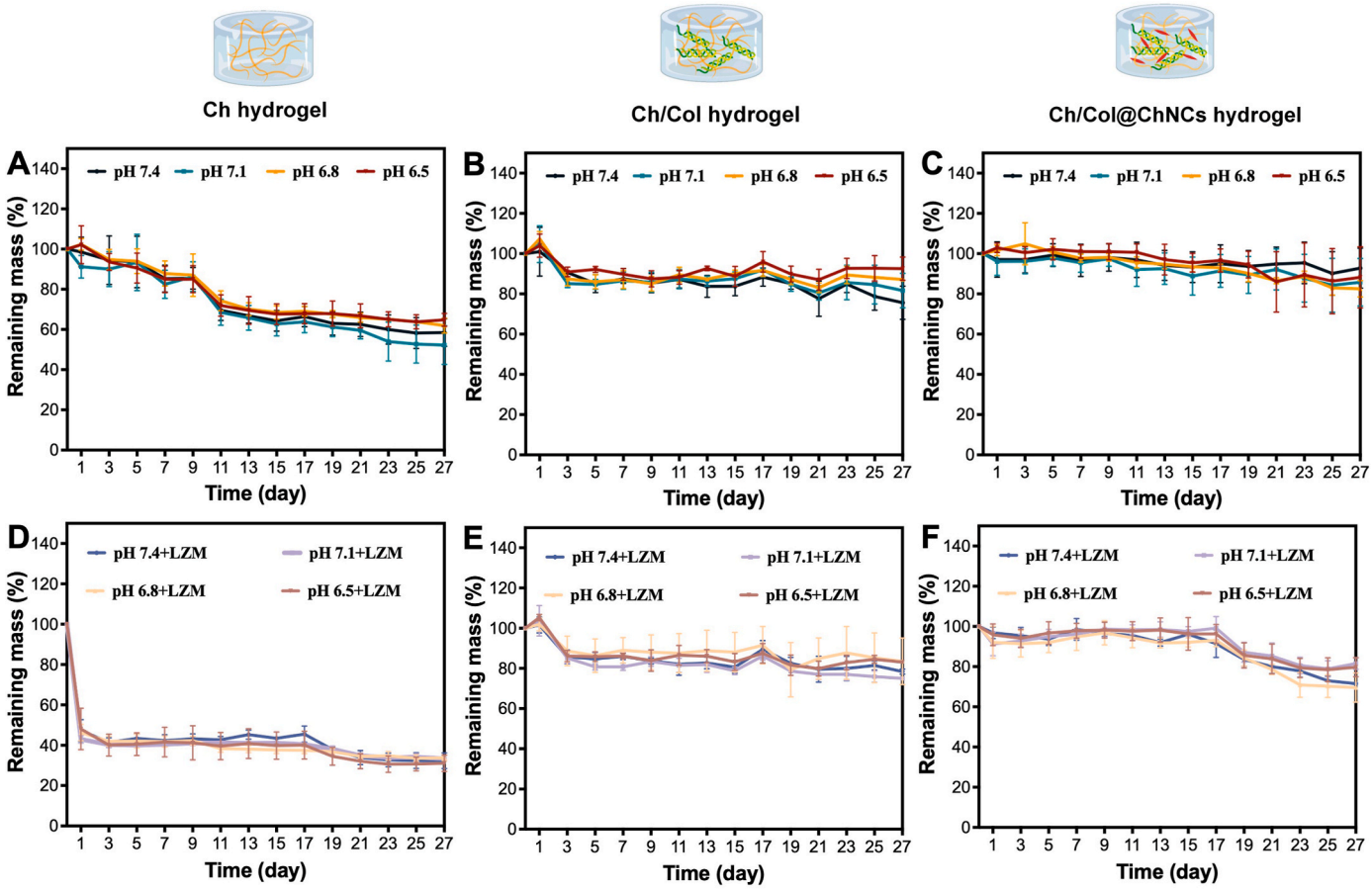

Fig. 5. Biodegradability of Ch-gel, Ch/Col-gel, and Ch/Col@ChNCs. (A, B, C) Degradation rates of Ch-gel, Ch/Col-gel, and Ch/Col@ChNCs-gel hydrogels in PBS simulated body fluid at different pH levels. (D, E, F) Degradation rates of Ch-gel, Ch/Col-gel, and Ch/Col@ChNCs-gel hydrogels in lysozyme-containing PBS simulating body fluid at different pH levels (n = 3).

3.8. Biocompatibility and ECM production of hAFCs co-cultured with hydrogel-patch

Human annulus fibrosus cells (hAFCs) were co-cultured within the composite hydrogels, and their proliferation was measured (Fig. 6C and D). On day 1, no significant differences were observed in cell viability across all groups, including the control, indicating similar initial integration of AF cells with the scaffolds. By day 3, cell viability in the control group increased to 2.1 times the initial level, reflecting the expected progression of AF cell activity under standard conditions. In contrast, the Ch/Col@ChNCs hydrogel demonstrated a remarkable increase in cell viability to 5.8 times the initial value. Additionally, Ch-gel and Ch/Col-gel supported varying degrees of cell proliferation due to their biocompatible 3D structures, which facilitate cell attachment [65]. By day 7, cell viability in the control group increased to six times the initial value, indicating a sustained positive proliferation response. Notably, the Ch/Col@ChNCs hydrogel exhibited continuous improvement, with cell viability reaching 10.3 times the initial value, demonstrating its superior biocompatibility.

Ch hydrogels are widely used as cell culture scaffolds due to their biocompatible 3D structure. Col contains specific cell adhesion motifs, such as the arginylglycylaspartic acid (RGD) sequence [66], which bind to integrins on the cell surface and activate signaling pathways such as focal adhesion kinase and extracellular signal-regulated kinase, promoting cell proliferation [67,68]. Thus, the Ch/Col@ChNCs hydrogel supports AF cell proliferation, confirming its excellent cellular compatibility and potential for tissue engineering applications.

The nanoscale size of chitin nanocrystals (ChNCs) provides distinct advantages over traditional chitin (Ch) particles. First, their increased surface area enhances the inherent positive charge of Ch, which, As the only natural polysaccharide with this property, can attract negatively charged cells to Ch-gel [69]. The expanded surface area also offers more adhesion points, facilitating interactions between cells and biomolecules that are essential for cell growth and proliferation, thereby improving bioactivity and overall efficacy [70]. Furthermore, the mechanical properties of the hydrogel matrix significantly influence cell behavior [71]. The unique crystalline structure of ChNCs improves the mechanical properties of the materials, thereby promoting surface cell proliferation [72]. The Ch/Col@ChNCs hydrogel provides a complex 3D microenvironment, as confirmed by SEM analysis. This interconnected structure fosters a supportive environment for cell infiltration, proliferation, and migration, effectively enhancing the number and activity of surface cells. These findings highlight the critical role of the implanted material in promoting AF tissue healing in vivo.

hAFCs were cultured on the prepared hydrogel in a 2D system (Fig. 6E). Immunofluorescence analysis was conducted to detect ECM expression levels in hAFCs grown on the Ch/Col@ChNCs hydrogel. As shown in Fig. 6F, no pink fluorescence of type II collagen (COL-II) was observed around the nuclei of hAFCs in the control group. In contrast, a substantial distribution of pink fluorescence, indicative of COL-II expression, was observed within the cells cultured on the Ch/Col@ChNCs hydrogel. This demonstrates that Ch/Col@ChNCs effectively enhance ECM COL-II protein expression in hAFCs. Thus, in vitro cell experiments highlight the effectiveness of this material in promoting AF repair.

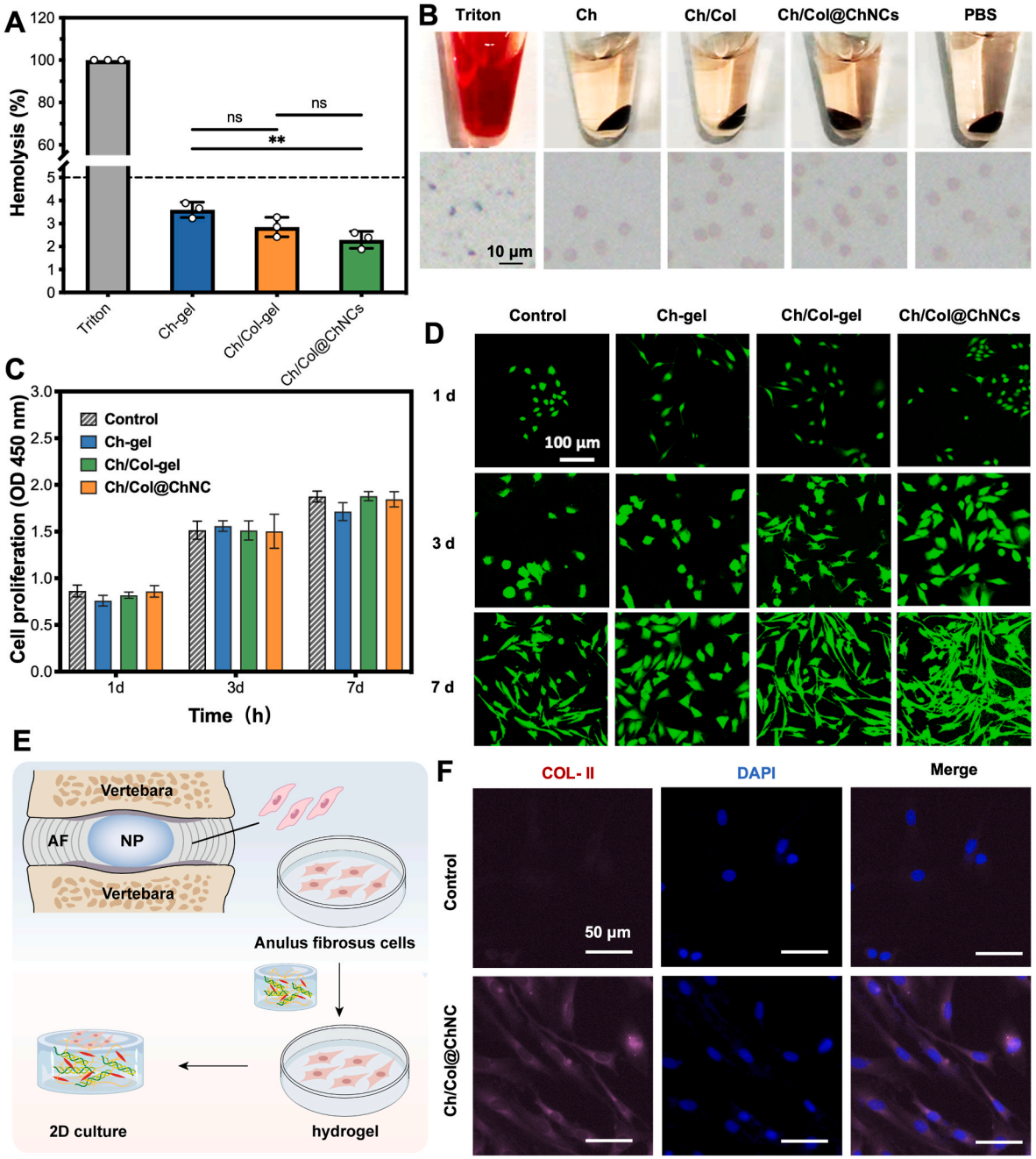

Fig. 6. In vitro cell compatibility experiments. (A) Hemolysis assay results and (B) optical microscopy images of the red blood cell (scale bar = 10 μm) s. (C) Cell viability and proliferation of hAFCs on different hydrogels measured using CCK-8 assay at days 1, 3, and 7. (D) Live/dead cell staining on days 1, 3, and 7 to demonstrate cell proliferation (green) on the hydrogels (scale bar = 100 μm). (E) Human annulus fibrosus cells (hAFCs) were obtained from human fibrous ring tissue and co-cultured with the prepared hydrogel in a 2D system. (F) Immunofluorescence staining showing hAFCs promoting Col deposition on Ch/Col@ChNCs (purple) (scale bar = 50 μm),(n = 3). Data are shown as mean ± SD; *$p < 0.05$, **$p < 0.01$, ***$p < 0.001$, ****$p < 0.0001$.

3.9. MRI analysis

The repair effectiveness of Ch/Col@ChNCs was evaluated by affixing a small hydrogel piece to AF defect with medical glue after disc puncture. MRI scans were performed at three, six, and nine weeks. New Zealand white rabbits were chosen as the model species because their spine anatomy, lacking the upright characteristics of the human spine, makes them suitable for puncture injury modeling (Fig. 7A–C).

MRI images provided a preliminary assessment of the in vivo repair effectiveness of Ch/Col@ChNCs by observing signal intensity and structural changes in NP. The modified Pfirrmann grading system (Table S1) was employed for scoring. This MRI-based classification method standardizes the evaluation of disc degeneration By assessing signal intensity and structural integrity. Using this system ensures consistency in analyzing therapeutic efficacy and facilitates quantitative comparisons with results from previous studies. These standardized evaluations are critical for validating the clinical relevance of Ch/Col@ChNCs and its potential as a biomaterial for annulus fibrosus repair. As shown in Fig. 7D, NP tissue in the intact control group consistently appeared as a high signal (white), indicating preserved highwater content and physiological activity without signs of degradation. In the untreated group, the NP tissue exhibited a non-uniform texture and appeared as a low signal, indicating degeneration with no improvements from weeks 3–9. This observation highlights the

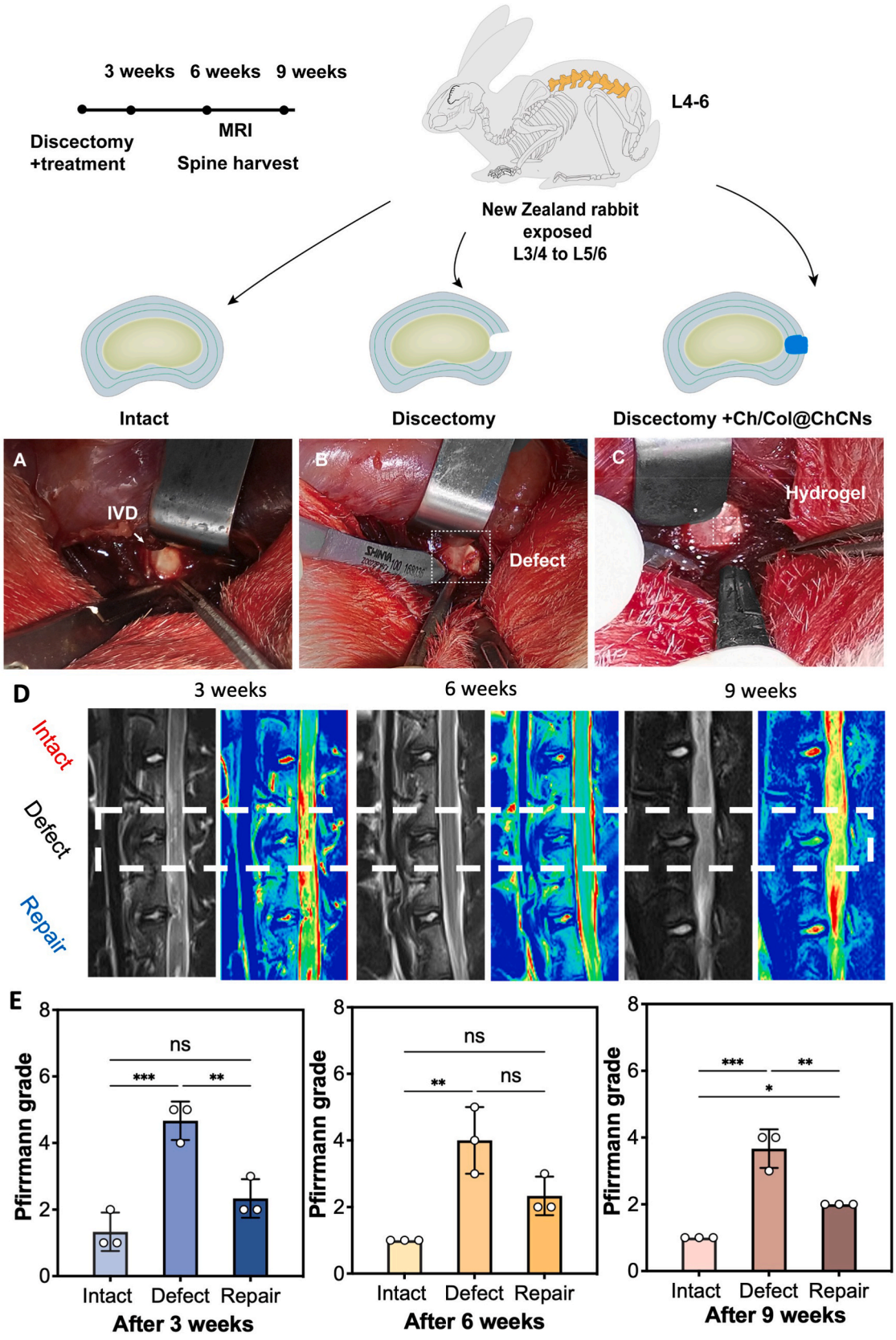

Fig. 7. Evaluation of hydrogel repair effects in vivo in New Zealand white rabbits. (A) IVDs exposed via an anterior-psoas lateral approach to the lumbar spine. (B) For IVDs receiving puncture injury, the AF tissue was punctured, and a portion of the NP tissue was aspirated. (C) IVDs treated with Ch/Col @ChNCs repair. (D) MRI images obtained after 3, 6, and 9 weeks. (E) Pfirrmann grade obtained after 3, 6, and 9 weeks. (n = 3). Data are shown as mean ± SD; *$p < 0.05$, **$p < 0.01$, ***$p < 0.001$, ****$p < 0.0001$.

progressive degenerative trajectory in the absence of treatment. In contrast, NP tissue in the Ch/Col@ChNCs group displayed a uniform white texture and a relatively intact structure. Although the signal intensity was slightly lower than that of the control group, both signal strength and tissue integrity were significantly higher than those in the untreated group. These results indicate that the implantation of Ch/Col@ChNCs preserved the physiological hydration state within the NP region, effectively mitigating degeneration. Based on the modified Foreman grading scores (Fig. 7E), Ch/Col@ChNCs repair achieved a lower IVD Foreman grade.

The repair observed with Ch/Col@ChNCs can be attributed to several key factors. First, the highly ordered crystalline structure of ChNCs enhanced the mechanical strength of the Ch/Col@ChNCs hydrogel, enabling IVD to maintain its original pressure and prevent further tissue damage. Additionally, Col and Ch are biocompatible materials that seamlessly integrate with natural tissues. The surface properties and 3D structure of ChNCs improve cell adhesion, while Col facilitates cell proliferation and deposition. Together, these properties support post-surgical AF tissue healing and prevent further NP moisture loss.

Ch/Col@ChNCs function on two levels: providing macroscopic mechanical support and promoting microscopic cellular proliferation. This dual-action mechanism drives IVD growth and repair. MRI results demonstrated that both signal strength and tissue integrity in the Ch/Col@ChNCs-treated group were significantly superior to those in the untreated group, confirming the in vivo effectiveness of this hydrogel. These findings highlight the potential of Ch/Col@ChNCs and highlight their potential for clinical applications in IVD repair.

3.10. Histological analysis

Histological analyses were performed at the defect site to assess the effectiveness of the repair interventions. Fig. 8A–C presents schematic illustrations depicting a healthy, intact intervertebral disc, the induced defect, and the repaired state with a hydrogel patch (blue). HE-stained sections (Fig. 8D–F) provided a comprehensive overview of tissue structure, cellular changes, and immune response within the IVD. In Fig. 8D, dense, pink-stained collagen in the AF and a uniform NP indicate no damage or signs of inflammation. Conversely, Fig. 8E reveals a clear gap in the AF structure, characterized by disruption and reduced tissue density. Fig. 8F demonstrates defect filling by the hydrogel patch, restoring AF continuity. The minimal inflammatory cell infiltration observed suggests a mild immune response [24].

Safranin O-Fast Green sections (Fig. 8G–I) specifically highlight proteoglycan distribution and matrix integrity. Fig. 8G reveals strong, uniform red staining in the AF and NP, indicating high proteoglycan content [73]. In contrast, Fig. 8H shows significant proteoglycan loss at the injury site, characterized by reduced staining and matrix disruption. Fig. 8I demonstrates restored red staining at the defect site, suggesting increased proteoglycan levels and partial matrix recovery, which reflect successful hydrogel integration. Notably, the hydrogel appears to promote ECM production in the AF, consistent with findings from in vitro cell experiments.Masson-stained sections (Fig. 8J–L) provide insights into collagen integrity and fibrosis. Fig. 8J shows dense blue staining in the AF, indicating normal collagen distribution and structural integrity. In Fig. 8K, a marked absence of blue staining at the injury site signifies collagen disruption and structural damage. In contrast, Fig. 8L highlights regenerated collagen with uniform blue staining, indicating successful hydrogel patch integration and controlled fibrosis, underscoring collagen-specific restoration.

The Ch/Col@ChNCs hydrogel demonstrates a greater number of intersection points and a more complex network structure, facilitating cell infiltration, proliferation, and migration. This architecture better mimics the microenvironment of the natural IVD. Additionally, Col interacts with specific receptors on the cell surface, promoting cell proliferation and adhesion to support the formation of new tissue. the

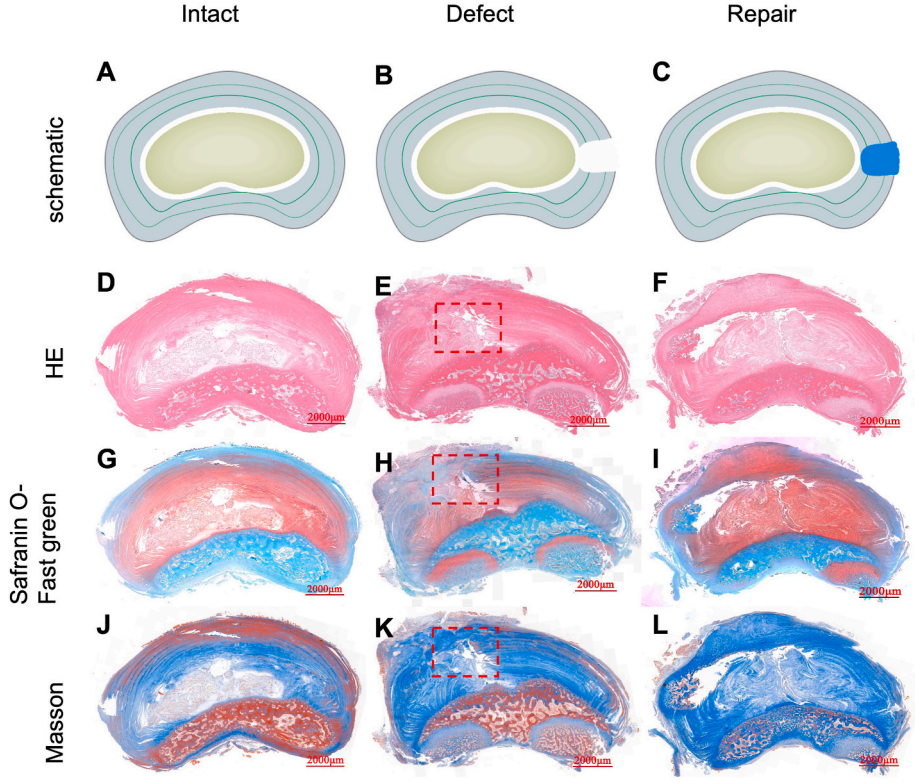

Fig. 8. Six-week histological evaluation results of IVDs. (A, B, C) Schematic of the intact (control), untreated, and treated IVDs. (D, E, F) Representative HE histological sections. (G, H, I) Representative safranin O- fast green histological sections. The red and green color refers to the cartilage and bone formation, respectively. (J, K, L) Representative bright-field Masson histological sections. The blue color refers to the Col fibers (scale bar = 2000 μm).

combined effects of Ch, Col, and ChNCs facilitate tissue regeneration and partially restore the hydration function of the IVD.

4. Discussion

Discectomy remains a widely utilized procedure for managing herniated intervertebral discs; however, repairing AF defects following surgery remains a significant clinical challenge [9,10]. Existing AF repair materials, such as sutures and metallic implants, provide temporary closure of defects but fail to effectively promote AF tissue regeneration [11,12]. The limitations of current biomaterials, including insufficient mechanical strength, suboptimal biocompatibility, and complex fabrication processes, restrict their broader adoption in clinical practice [11]. This study presents a novel composite hydrogel, integrating Ch, Col, and ChNCs, designed to enhance the mechanical properties and cell compatibility of the material, thereby promoting AF tissue regeneration and repair.

Materials developed for post-surgical AF defect repair must exhibit mechanical properties closely aligned with those of native tissue to endure physiological mechanical stresses [31]. The combination of Col and Ch in hydrogel form represents a promising biomedical material, as Col, a natural component of AF tissue, provides excellent biological compatibility [30]. However, the gel matrix formed by non-covalent interactions between Col molecules is inherently soft and fails to meet the stringent mechanical demands of AF tissue. ChNCs were incorporated into the hydrogel matrix to create a Ch/Col@ChNCs composite hydrogel patch to address this limitation. This composite hydrogel demonstrates a compression modulus of 0.27 MPa, closely matching the reported values for cellulose nanocrystal-reinforced hydrogels (approximately 0.3 MPa). Furthermore, the composite achieves a maximum compressive strength of 1.45 MPa, significantly exceeding that of cellulose nanocrystal-reinforced hydrogels (approximately 0.46 MPa) [25]. These enhanced mechanical properties ensure the structural integrity of the hydrogel under intradiscal pressure, effectively mimicking the mechanical characteristics required for AF tissue repair.

In addition, compared to previously reported polycaprolactone (PCL)-based organized type I collagen patches [20], the Ch/Col@ChNCs hydrogel demonstrated superior water absorption. This property is critical for maintaining disc hydration, thereby preventing further NP dehydration and degeneration. Despite its impressive mechanical strength and water retention capabilities, the material exhibits relatively low adhesive strength, necessitating the use of medical adhesives to secure it to AF tissue. Unlike other bioadhesives used in AF repair [74], the Ch/Col@ChNCs composite lacks intrinsic adhesiveness. However, applying medical adhesives mitigates challenges such as unwanted adhesion to surgical instruments, thereby reducing procedural complexity. Additionally, the fabrication process of this hydrogel patch is simpler than other reported approaches, enhancing its potential for clinical translation—another distinct advantage of this material.

In vitro cell experiments further confirmed the excellent biocompatibility of the composite hydrogel. This material is intended for post-surgical tissue repair and is designed to interact directly with blood cells. Experimental findings demonstrated that the Ch/Col@ChNCs hydrogel exhibits high hemocompatibility, ensuring its safe application in clinical settings. Additionally, the hydrogel does not inhibit AF cell proliferation, highlighting its outstanding biocompatibility, consistent with previously reported biomaterials. Notably, the hydrogel patch significantly enhances ECM production. Scanning electron microscopy (SEM) revealed its porous structure, which provides an ideal three-dimensional scaffold for cell adhesion, migration, and proliferation. This porous architecture shows strong potential for promoting tissue regeneration in vitro. compared to traditional materials [11], Ch/Col@ChNCs demonstrated superior efficacy in enhancing cell activity and supporting tissue remodeling.

To further evaluate in vivo reparative efficacy of the material, a rabbit IVD puncture defect model was employed. Compared to commonly used rodent models, rabbit IVDs are closer in size and physiological structure to human discs, with mechanical loading conditions that more accurately reflect clinical scenarios. Additionally, the larger size of the rabbit model allows for a more realistic assessment of the performance of the material under in vivo conditions [40]. The increased disc size also provides more reliable data, particularly when evaluating the long-term stability and tissue integration of the material. This model effectively replicates the biomechanical environment of an IVD defect, enhancing the findings' clinical relevance. Experimental results demonstrated that the Ch/Col@ChNCs composite hydrogel effectively repaired AF defects and maintained NP hydration post-surgery, preventing further degeneration. MRI and histological analyses revealed that after 6–9 weeks of repair, the hydrogel formed a structure in the defect area that closely resembled native tissue. Compared to the untreated group, the Ch/Col@ChNCs group exhibited significant improvements in both AF and NP structural integrity. These findings indicate that the Ch/Col@ChNCs composite hydrogel not only effectively seals AF defects but also preserves disc function over an extended period, preventing post-surgical degeneration.

Nonetheless, several challenges must still be addressed. First, the low adhesive strength of the material could introduce complexity during clinical application, underscoring the need for further research to enhance its adhesive properties. Second, while the material exhibited favorable degradation characteristics in both in vitro and in vivo studies, its long-term stability in larger animal models remains to be thoroughly investigated. Future studies should prioritize evaluating the performance of the material under diverse physiological loads and environmental conditions to ensure its broad applicability in clinical settings. Additionally, the underlying mechanisms driving tissue repair should be explored in greater detail to optimize the material further for clinical use.

5. Conclusion

This study demonstrated the successful preparation of Ch/Col@ChNCs using a simple fabrication process to repair damaged annulus fibrosus (AF) following discectomy. The biomaterial exhibited excellent biocompatibility, owing to the inherent properties of chitin (Ch) and collagen (Col). The incorporation of chitin nanocrystals (ChNCs) significantly enhanced the mechanical strength of the hydrogel, reducing nucleus pulposus (NP) dehydration after AF rupture. With a compressive modulus of 0.27 MPa, Ch/Col@ChNCs provided sufficient mechanical support for the intervertebral disc (IVD) load-bearing conditions in a lying position post-discectomy. While Ch/Col@ChNCs show substantial potential for clinical applications in AF repair, further research should focus on optimizing its long-term stability and integration with native tissues. Evaluating its performance under varied mechanical loading conditions, understanding its role in immune environment regulation, and elucidating the mechanisms underlying cellular responses will offer deeper insights into its therapeutic potential and guide its clinical translation.

CRediT authorship contribution statement

Mingzhi Liu: Methodology, Formal analysis, Data curation. **Zhiyong Cui:** Writing – original draft, Visualization, Formal analysis, Data curation. **Derong Xu:** Methodology, Investigation. **Chenguang Liu:** Writing – review & editing, Supervision, Conceptualization. **Chuanli Zhou:** Supervision, Funding acquisition.

Funding

This work was supported by the Natural Science Foundation of Shandong Province [grant number ZR2021MH020]; the National Natural Science Foundation of China [grant numbers 82372478 and 82202751]; and Qingdao Science and Technology Benefiting the People

Special Project [grant numbers 2418smjk2nsh]. The funding bodies were not involved in the study design, data collection and analysis, manuscript preparation, and decision to publish.

Declaration of competing interest

The authors declare that they have no known competing financial interests or personal relationships that could have appeared to influence the work reported in this paper.

Acknowledgments

The author are grateful to the Laboratory of Biochemistry and Marine Biomaterials at Ocean University of China for providing the experimental platform, and also expresses gratitude to the School of Medicine at Qingdao University for offering the animal experimentation platform.

Appendix A. Supplementary data

Supplementary data to this article can be found online at https://doi.org/10.1016/j.mtbio.2025.101537.

Data availability

Data will be made available on request.

References

[1] S. Chen, M. Chen, X. Wu, S. Lin, C. Tao, H. Cao, Z. Shao, G. Xiao, Global, regional and national burden of low back pain 1990–2019: a systematic analysis of the Global Burden of Disease study 2019, Journal of Orthopaedic Translation 32 (2022) 49–58, https://doi.org/10.1016/j.jot.2021.07.005.

[2] N.N. Knezevic, K.D. Candido, J.W.S. Vlaeyen, J. Van Zundert, S.P. Cohen, Low back pain, Lancet 398 (2021) 78–92, https://doi.org/10.1016/S0140-6736(21)00733-9.

[3] A.M. El Melhat, A.S.A. Youssef, M.R. Zebdawi, M.A. Hafez, L.H. Khalil, D. E. Harrison, Non-surgical approaches to the management of lumbar disc herniation associated with radiculopathy: a narrative review, JCM 13 (2024) 974, https://doi.org/10.3390/jcm13040974.

[4] H.B. Albert, A.J. Sayari, J.N. Barajas, A.L. Hornung, G. Harada, M.T. Nolte, A. V. Chee, D. Samartzis, A. Tkachev, The impact of novel inflammation-preserving treatment towards lumbar disc herniation resorption in symptomatic patients: a prospective, multi-imaging and clinical outcomes study, Eur. Spine J. 33 (2024) 964–973, https://doi.org/10.1007/s00586-023-08064-x.

[5] R.A. Deyo, S.K. Mirza, Herniated lumbar intervertebral disk, N. Engl. J. Med. 374 (2016) 1763–1772, https://doi.org/10.1056/NEJMcp1512658.

[6] T.T. Hickman, S. Rathan-Kumar, S.H. Peck, Development, pathogenesis, and regeneration of the intervertebral disc: current and future insights spanning traditional to omics methods, Front. Cell Dev. Biol. 10 (2022) 841831, https://doi.org/10.3389/fcell.2022.841831.

[7] I.L. Mohd Isa, S.L. Teoh, N.H. Mohd Nor, S.A. Mokhtar, Discogenic low back pain: anatomy, pathophysiology and treatments of intervertebral disc degeneration, IJMS 24 (2022) 208, https://doi.org/10.3390/ijms24010208.

[8] P.H. Wu, H.S. Kim, I.-T. Jang, Intervertebral disc diseases part 2: a review of the current diagnostic and treatment strategies for intervertebral disc disease, IJMS 21 (2020) 2135, https://doi.org/10.3390/ijms21062135.

[9] A.S. Chung, B. McKnight, J.C. Wang, Scientific view on endoscopic spine surgery: can spinal endoscopy become a mainstream surgical tool? World Neurosurgery 145 (2021) 708–711, https://doi.org/10.1016/j.wneu.2020.05.238.

[10] F. Wang, K. Chen, Q. Lin, Y. Ma, H. Huang, C. Wang, P. Zhou, Earlier or heavier spinal loading is more likely to lead to recurrent lumbar disc herniation after percutaneous endoscopic lumbar discectomy, J. Orthop. Surg. Res. 17 (2022) 356, https://doi.org/10.1186/s13018-022-03242-x.

[11] Y. Ying, K. Cai, X. Cai, K. Zhang, R. Qiu, G. Jiang, K. Luo, Recent advances in the repair of degenerative intervertebral disc for preclinical applications, Front. Bioeng. Biotechnol. 11 (2023) 1259731, https://doi.org/10.3389/fbioe.2023.1259731.

[12] On behalf of the Annular Closure RCT Study Group, J.C. Kienzler, P.D. Klassen, L. E. Miller, R. Assaker, V. Heidecke, S. Fröhlich, C. Thomé, Three-year results from a randomized trial of lumbar discectomy with annulus fibrosus occlusion in patients at high risk for reherniation, Acta Neurochir. 161 (2019) 1389–1396, https://doi.org/10.1007/s00701-019-03948-8.

[13] W.J. Choy, K. Phan, A.D. Diwan, C.S. Ong, R.J. Mobbs, Annular closure device for disc herniation: meta-analysis of clinical outcome and complications, BMC Musculoskelet Disord 19 (2018) 290, https://doi.org/10.1186/s12891-018-2213-5.

[14] K. Zheng, D. Du, Recent advances of hydrogel-based biomaterials for intervertebral disc tissue treatment: a literature review, J Tissue Eng Regen Med 15 (2021) 299–321, https://doi.org/10.1002/term.3172.

[15] A. Zhang, Z. Cheng, Y. Chen, P. Shi, W. Gan, Y. Zhang, Emerging tissue engineering strategies for annulus fibrosus therapy, Acta Biomater. 167 (2023) 1–15, https://doi.org/10.1016/j.actbio.2023.06.012.

[16] S.R. Sloan, C. Wipplinger, S. Kirnaz, R. Navarro-Ramirez, F. Schmidt, D. McCloskey, T. Pannellini, A. Schiavinato, R. Härtl, L.J. Bonassar, Combined nucleus pulposus augmentation and annulus fibrosus repair prevents acute intervertebral disc degeneration after discectomy, Sci. Transl. Med. 12 (2020), https://doi.org/10.1126/scitranslmed.aay2380 eaay2380.

[17] X. Li, R. Huo, L. Li, H. Cherif, X. Lan, M.H. Weber, L. Haglund, J. Li, Composite hydrogel sealants for annulus fibrosus repair, ACS Biomater. Sci. Eng. 10 (2024) 5094–5107, https://doi.org/10.1021/acsbiomaterials.4c00548.

[18] Z. Du, L. Zhu, A heterologous fibrin glue enhances the closure effect of surgical suture on the repair of annulus fibrous defect in a sheep model, CURR MED SCI 39 (2019) 597–603, https://doi.org/10.1007/s11596-019-2079-2.

[19] M.R. Saghari Fard, J.P. Krueger, S. Stich, P. Berger, A.A. Kühl, M. Sittinger, T. Hartwig, M. Endres, A biodegradable polymeric matrix for the repair of annulus fibrosus defects in intervertebral discs, Tissue Eng Regen Med 19 (2022) 1311–1320, https://doi.org/10.1007/s13770-022-00466-0.

[20] A. Dewle, P. Rakshasmare, A. Srivastava, A polycaprolactone (PCL)-Supported electrocompacted aligned collagen type-I patch for annulus fibrosus repair and regeneration, ACS Appl. Bio Mater. 4 (2021) 1238–1251, https://doi.org/10.1021/acsabm.0c01084.

[21] Z. Tu, F. Han, Z. Zhu, Q. Yu, C. Liu, Y. Bao, B. Li, F. Zhou, Sustained release of basic fibroblast growth factor in micro/nanofibrous scaffolds promotes annulus fibrosus regeneration, Acta Biomater. 166 (2023) 241–253, https://doi.org/10.1016/j.actbio.2023.05.034.

[22] S.R. Sloan, M. Lintz, I. Hussain, R. Hartl, L.J. Bonassar, Biologic annulus fibrosus repair: a review of preclinical *in vivo* investigations, Tissue Eng. B Rev. 24 (2018) 179–190, https://doi.org/10.1089/ten.teb.2017.0351.

[23] Y. Wang, C. Zheng, Y. Wu, B. Zhang, C. Hu, C. Guo, Q. Kong, Y. Wang, An injectable and self-strengthening nanogel encapsuled hydrogel gene delivery system promotes degenerative nucleus pulposus repair, Compos. B Eng. 250 (2023) 110469, https://doi.org/10.1016/j.compositesb.2022.110469.

[24] F. Han, Z. Tu, Z. Zhu, D. Liu, Q. Meng, Q. Yu, Y. Wang, J. Chen, T. Liu, F. Han, B. Li, Targeting endogenous reactive oxygen species removal and regulating regenerative microenvironment at annulus fibrosus defects promote tissue repair, ACS Nano 17 (2023) 7645–7661, https://doi.org/10.1021/acsnano.3c00093.

[25] I. Doench, T. Ahn Tran, L. David, A. Montembault, E. Viguier, C. Gorzelanny, G. Sudre, T. Cachon, M. Louback-Mohamed, N. Horbelt, C. Peniche-Covas, A. Osorio-Madrazo, Cellulose nanofiber-reinforced chitosan hydrogel composites for intervertebral disc tissue repair, Biomimetics 4 (2019) 19, https://doi.org/10.3390/biomimetics4010019.

[26] R. Ye, S. Liu, W. Zhu, Y. Li, L. Huang, G. Zhang, Y. Zhang, Synthesis, characterization, properties, and biomedical application of chitosan-based hydrogels, Polymers 15 (2023) 2482, https://doi.org/10.3390/polym15112482.

[27] S. Lee, L.T. Hao, J. Park, D.X. Oh, D.S. Hwang, Nanochitin and nanochitosan: chitin nanostructure engineering with multiscale properties for biomedical and environmental applications, Adv. Mater. 35 (2023) 2203325, https://doi.org/10.1002/adma.202203325.

[28] L. Li, K. Liu, J. Chen, W. Wen, H. Li, L. Li, S. Ding, M. Liu, C. Zhou, B. Luo, Bone ECM-inspired biomineralization chitin whisker liquid crystal hydrogels for bone regeneration, Int. J. Biol. Macromol. 231 (2023) 123335, https://doi.org/10.1016/j.ijbiomac.2023.123335.

[29] F. Koohzad, A. Asoodeh, Cross-linked electrospun pH-sensitive nanofibers adsorbed with temporin-Ra for promoting wound healing, ACS Appl. Mater. Interfaces 15 (2023) 15172–15184, https://doi.org/10.1021/acsami.2c23268.

[30] M. Zheng, X. Wang, Y. Chen, O. Yue, Z. Bai, B. Cui, H. Jiang, X. Liu, A review of recent progress on collagen-based biomaterials, Adv. Healthcare Mater. 12 (2023) 2202042, https://doi.org/10.1002/adhm.202202042.

[31] D. Zhou, H. Liu, Z. Zheng, D. Wu, Design principles in mechanically adaptable biomaterials for repairing annulus fibrosus rupture: a review, Bioact. Mater. 31 (2024) 422–439, https://doi.org/10.1016/j.bioactmat.2023.08.012.

[32] M. Yanat, K. Schroën, Advances in chitin-based nanoparticle use in biodegradable polymers: a review, Carbohydr. Polym. 312 (2023) 120789, https://doi.org/10.1016/j.carbpol.2023.120789.

[33] J. Araki, Y. Yamanaka, K. Ohkawa, Chitin-chitosan nanocomposite gels: reinforcement of chitosan hydrogels with rod-like chitin nanowhiskers, Polym. J. 44 (2012) 713–717, https://doi.org/10.1038/pj.2012.11.

[34] Q. Zhang, P. Sun, Z. Xu, W. Qu, Y. Zhang, X. Sui, Chitin nanocrystals as natural gel modifier for yielding stronger acid-induced soy protein isolate gel, Carbohydr. Polym. 323 (2024) 121446, https://doi.org/10.1016/j.carbpol.2023.121446.

[35] F. Xing, Z. Chi, R. Yang, D. Xu, J. Cui, Y. Huang, C. Zhou, C. Liu, Chitin-hydroxyapatite-collagen composite scaffolds for bone regeneration, Int. J. Biol. Macromol. 184 (2021) 170–180, https://doi.org/10.1016/j.ijbiomac.2021.05.019.

[36] M.R. Barkhordari, M. Fathi, Production and characterization of chitin nanocrystals from prawn shell and their application for stabilization of Pickering emulsions, Food Hydrocolloids 82 (2018) 338–345, https://doi.org/10.1016/j.foodhyd.2018.04.030.

[37] H.-S. Jung, H.C. Kim, W. Ho Park, Robust methylcellulose hydrogels reinforced with chitin nanocrystals, Carbohydr. Polym. 213 (2019) 311–319, https://doi.org/10.1016/j.carbpol.2019.03.009.

[38] B. Qiao, J. Wang, L. Qiao, A. Maleki, Y. Liang, B. Guo, ROS-responsive hydrogels with spatiotemporally sequential delivery of antibacterial and anti-inflammatory

drugs for the repair of MRSA-infected wounds, Regenerative Biomaterials 11 (2024) rbad110, https://doi.org/10.1093/rb/rbad110.
[39] T. Lei, Y. Zhang, Q. Zhou, X. Luo, K. Tang, R. Chen, C. Yu, Z. Quan, A Novel Approach for the Annulus Needle Puncture Model of Intervertebral Disc Degeneration in Rabbits, (n.d.).
[40] M. Zhang, Y. Li, W. Wang, Y. Yang, X. Shi, M. Sun, Y. Hao, Y. Li, Comparison of physicochemical and rheology properties of Shiitake stipes-derived chitin nanocrystals and nanofibers, Carbohydr. Polym. 244 (2020) 116468, https://doi.org/10.1016/j.carbpol.2020.116468.
[41] N. Naseri, C. Algan, V. Jacobs, M. John, K. Oksman, A.P. Mathew, Electrospun chitosan-based nanocomposite mats reinforced with chitin nanocrystals for wound dressing, Carbohydr. Polym. 109 (2014) 7–15, https://doi.org/10.1016/j.carbpol.2014.03.031.
[42] M. Yanat, I. Colijn, K. Schroën, Chitin nanocrystals provide antioxidant activity to polylactic acid films, Polymers 14 (2022) 2965, https://doi.org/10.3390/polym14142965.
[43] S. Liu, Y. Chen, C. Liu, L. Gan, X. Ma, J. Huang, Polydopamine-coated cellulose nanocrystals as an active ingredient in poly(vinyl alcohol) films towards intensifying packaging application potential, Cellulose 26 (2019) 9599–9612, https://doi.org/10.1007/s10570-019-02749-7.
[44] N. Lin, S. Zhao, L. Gan, P.R. Chang, T. Xia, J. Huang, Preparation of fungus-derived chitin nanocrystals and their dispersion stability evaluation in aqueous media, Carbohydr. Polym. 173 (2017) 610–618, https://doi.org/10.1016/j.carbpol.2017.06.016.
[45] Y. Fan, T. Saito, A. Isogai, Individual chitin nano-whiskers prepared from partially deacetylated α-chitin by fibril surface cationization, Carbohydr. Polym. 79 (2010) 1046–1051, https://doi.org/10.1016/j.carbpol.2009.10.044.
[46] M. Liu, H. Zheng, J. Chen, S. Li, J. Huang, C. Zhou, Chitosan-chitin nanocrystal composite scaffolds for tissue engineering, Carbohydr. Polym. 152 (2016) 832–840, https://doi.org/10.1016/j.carbpol.2016.07.042.
[47] M.B. Nair, G. Baranwal, P. Vijayan, K.S. Keyan, R. Jayakumar, Composite hydrogel of chitosan–poly(hydroxybutyrate- co -valerate) with chondroitin sulfate nanoparticles for nucleus pulposus tissue engineering, Colloids Surf. B Biointerfaces 136 (2015) 84–92, https://doi.org/10.1016/j.colsurfb.2015.08.026.
[48] Y. Yang, J. Cui, M. Zheng, C. Hu, S. Tan, Y. Xiao, Q. Yang, Y. Liu, One-step synthesis of amino-functionalized fluorescent carbon nanoparticles by hydrothermal carbonization of chitosan, Chem. Commun. 48 (2012) 380–382, https://doi.org/10.1039/C1CC15678K.
[49] M. Liu, J. Huang, B. Luo, C. Zhou, Tough and highly stretchable polyacrylamide nanocomposite hydrogels with chitin nanocrystals, Int. J. Biol. Macromol. 78 (2015) 23–31, https://doi.org/10.1016/j.ijbiomac.2015.03.059.
[50] L. Xu, H. Kang, W. Wei, T. Goto, X. Wu, H. Dai, Freezing, salting-out and mineralization — a simple, universal and modular strategy for constructing mineralized hydrogels, Adv. Funct. Mater. 34 (2024) 2406367, https://doi.org/10.1002/adfm.202406367.
[51] H. Moon, S. Choy, Y. Park, Y.M. Jung, J.M. Koo, D.S. Hwang, Different molecular interaction between collagen and α- or β-chitin in mechanically improved electrospun composite, Mar. Drugs 17 (2019) 318, https://doi.org/10.3390/md17060318.
[52] L. Fu, L. Li, Q. Bian, B. Xue, J. Jin, J. Li, Y. Cao, Q. Jiang, H. Li, Cartilage-like protein hydrogels engineered via entanglement, Nature 618 (2023) 740–747, https://doi.org/10.1038/s41586-023-06037-0.
[53] B.Y.S. Kumar, A.M. Isloor, G.C.M. Kumar, Inamuddin, A.M. Asiri, Nanohydroxyapatite reinforced chitosan composite hydrogel with tunable mechanical and biological properties for cartilage regeneration, Sci. Rep. 9 (2019) 15957, https://doi.org/10.1038/s41598-019-52042-7.
[54] D. Sun, Y. Gao, Y. Zhou, M. Yang, J. Hu, T. Lu, T. Wang, Enhance fracture toughness and fatigue resistance of hydrogels by reversible alignment of nanofibers, ACS Appl. Mater. Interfaces 14 (2022) 49389–49397, https://doi.org/10.1021/acsami.2c16273.
[55] X. Zhao, X. Chen, H. Yuk, S. Lin, X. Liu, G. Parada, Soft materials by design: unconventional polymer networks give extreme properties, Chem. Rev. 121 (2021) 4309–4372, https://doi.org/10.1021/acs.chemrev.0c01088.
[56] R. Jayakumar, M. Prabaharan, R.L. Reis, J.F. Mano, Graft copolymerized chitosan—present status and applications, Carbohydr. Polym. 62 (2005) 142–158, https://doi.org/10.1016/j.carbpol.2005.07.017.
[57] L. Jiang, X. Huang, C. Tian, Y. Zhong, M. Yan, C. Miao, T. Wu, X. Zhou, Preparation and characterization of porous cellulose acetate nanofiber hydrogels, Gels 9 (2023) 484, https://doi.org/10.3390/gels9060484.
[58] T. Jayaramudu, H.-U. Ko, H.C. Kim, J.W. Kim, J. Kim, Swelling behavior of polyacrylamide–cellulose nanocrystal hydrogels: swelling kinetics, temperature, and pH effects, Materials 12 (2019) 2080, https://doi.org/10.3390/ma12132080.
[59] B. Bi, H. Liu, W. Kang, R. Zhuo, X. Jiang, An injectable enzymatically crosslinked tyramine-modified carboxymethyl chitin hydrogel for biomedical applications, Colloids Surf. B Biointerfaces 175 (2019) 614–624, https://doi.org/10.1016/j.colsurfb.2018.12.029.
[60] F. Li, Q. Ba, S. Niu, Y. Guo, Y. Duan, P. Zhao, C. Lin, J. Sun, In-situ forming biodegradable glycol chitosan-based hydrogels: synthesis, characterization, and chondrocyte culture, Mater. Sci. Eng. C 32 (2012) 2017–2025, https://doi.org/10.1016/j.msec.2012.05.021.
[61] Y.-W. Cho, Y.-N. Cho, S.-H. Chung, G. Yoo, S.-W. Ko, Water-soluble Chitin as a Wound Healing Accelerator, (n.d.).
[62] G. Toader, I. Podaru, E. Rusen, A. Diacon, R. Ginghina, M. Alexandru, F. Zorila, A. Gavrila, B. Trica, T. Rotariu, M. Ionita, Nafcillin-loaded photocrosslinkable nanocomposite hydrogels for biomedical applications, Pharmaceutics 15 (2023) 1588, https://doi.org/10.3390/pharmaceutics15061588.
[63] Y. Wang, Y. Wu, B. Zhang, C. Zheng, C. Hu, C. Guo, Q. Kong, Y. Wang, Repair of degenerative nucleus pulposus by polyphenol nanosphere-encapsulated hydrogel gene delivery system, Biomaterials 298 (2023) 122132, https://doi.org/10.1016/j.biomaterials.2023.122132.
[64] D. Yuan, Z. Chen, X. Xiang, S. Deng, K. Liu, D. Xiao, L. Deng, G. Feng, The establishment and biological assessment of a whole tissue-engineered intervertebral disc with PBST fibers and a chitosan hydrogel *in vitro* and *in vivo*, J. Biomed. Mater. Res. 107 (2019) 2305–2316, https://doi.org/10.1002/jbm.b.34323.
[65] H. Wang, D. Wang, B. Luo, D. Wang, H. Jia, P. Peng, Q. Shang, J. Mao, C. Gao, Y. Peng, L. Gan, J. Du, Z. Luo, L. Yang, Decoding the annulus fibrosus cell atlas by scRNA-seq to develop an inducible composite hydrogel: a novel strategy for disc reconstruction, Bioact. Mater. 14 (2022) 350–363, https://doi.org/10.1016/j.bioactmat.2022.01.040.
[66] L. Yu, M. Wei, Biomineralization of collagen-based materials for hard tissue repair, IJMS 22 (2021) 944, https://doi.org/10.3390/ijms22020944.
[67] M.G. Jeschke, G. Sandmann, T. Schubert, D. Klein, Effect of oxidized regenerated cellulose/collagen matrix on dermal and epidermal healing and growth factors in an acute wound, Wound Repair Regen. 13 (2005) 324–331, https://doi.org/10.1111/j.1067-1927.2005.130316.x.
[68] J. Huang, S. Heng, W. Zhang, Y. Liu, T. Xia, C. Ji, L. Zhang, Dermal extracellular matrix molecules in skin development, homeostasis, wound regeneration and diseases, Semin. Cell Dev. Biol. 128 (2022) 137–144, https://doi.org/10.1016/j.semcdb.2022.02.027.
[69] M. Zhang, X. Qiao, W. Han, T. Jiang, F. Liu, X. Zhao, Alginate-chitosan oligosaccharide-ZnO composite hydrogel for accelerating wound healing, Carbohydr. Polym. 266 (2021) 118100, https://doi.org/10.1016/j.carbpol.2021.118100.
[70] G. Chang, Q. Dang, C. Liu, X. Wang, H. Song, H. Gao, H. Sun, B. Zhang, D. Cha, Carboxymethyl chitosan and carboxymethyl cellulose based self-healing hydrogel for accelerating diabetic wound healing, Carbohydr. Polym. 292 (2022) 119687, https://doi.org/10.1016/j.carbpol.2022.119687.
[71] P. Li, L. Fu, Z. Liao, Y. Peng, C. Ning, C. Gao, D. Zhang, X. Sui, Y. Lin, S. Liu, C. Hao, Q. Guo, Chitosan hydrogel/3D-printed poly(ε-caprolactone) hybrid scaffold containing synovial mesenchymal stem cells for cartilage regeneration based on tetrahedral framework nucleic acid recruitment, Biomaterials 278 (2021) 121131, https://doi.org/10.1016/j.biomaterials.2021.121131.
[72] S. Li, J. Liu, S. Liu, W. Jiao, X. Wang, Chitosan oligosaccharides packaged into rat adipose mesenchymal stem cells-derived extracellular vesicles facilitating cartilage injury repair and alleviating osteoarthritis, J. Nanobiotechnol. 19 (2021) 343, https://doi.org/10.1186/s12951-021-01086-x.
[73] M. Ul-Islam, W. Alhajaim, A. Fatima, S. Yasir, T. Kamal, Y. Abbas, S. Khan, A. H. Khan, S. Manan, M.W. Ullah, G. Yang, Development of low-cost bacterial cellulose-pomegranate peel extract-based antibacterial composite for potential biomedical applications, Int. J. Biol. Macromol. 231 (2023) 123269, https://doi.org/10.1016/j.ijbiomac.2023.123269.
[74] X. Li, Y. Liu, L. Li, R. Huo, F. Ghezelbash, Z. Ma, G. Bao, S. Liu, Z. Yang, M. H. Weber, N.Y.K. Li-Jessen, L. Haglund, J. Li, Tissue-mimetic hybrid bioadhesives for intervertebral disc repair, Mater. Horiz. 10 (2023) 1705–1718, https://doi.org/10.1039/D2MH01242A.